Designing, Building, and Testing of a Hybrid Wavefront Sensor for Adaptive Optics

Ryan J. Hamilton, Joseph A. Rice, Charlotte E. Guthery and Michael Hart

James C. Wyant College of Optical Sciences, The University of Arizona, 1630 E University Blvd, Tucson, AZ

ABSTRACT

A bench top prototype hybrid wavefront sensor (HyWFS) has been designed and built. The construction and initial tests are reported in this paper. The sensor creates four images of the optical system pupil generated by a pyramid prism placed in a focal plane of the telescope, analogous to a pyramid wavefront sensor (PyWFS). A lenslet array forms a spot pattern of beacon images from each pupil in the manner of a Shack-Hartmann wavefront sensor (SHWFS). The intent of this work was to validate the concept presented by Guthery and Hart[1] in a low-cost prototype. The images produced by the hybrid system can be interpreted as either PyWFS data, yielding high sensitivity wavefront reconstruction with low dynamic range, or as SHWFS data, offering wavefront reconstruction with characteristically lower sensitivity but a large dynamic range. The HyWFS retains the desirable properties of both types without modulating the image on the pyramid prism.[2] For an initial system test, Zernike modes and Kolmogorov phase maps are placed on a deformable mirror (DM) and imaged with the HyWFS in a laboratory. The collected initial test images are then used to develop the final test reconstruction software and test setup. Final test software and system alignment is currently underway at the University of Arizona.

Keywords: Wavefront Sensing, Hybrid Wavefront Sensor, Pyramid Wavefront Sensor, Shack-Hartmann Wavefront Sensor, Adaptive Optics

1. INTRODUCTION

The use of adaptive optics (AO) is essential for obtaining the full imaging potential for present large aperture telescopes. AO is of even greater importance for the upcoming extremely large telescopes (ELTs). The bigger apertures and more challenging science goals demand AO correction with high sensitivity and high dynamic range. Wavefront sensing that achieves both is therefore essential; the HyWFS described here offers a solution that is straightforward to implement, and unlike the modulated PyWFS that is now in use at a number of telescopes, requires no moving parts.

Cophasing large segmented aperture telescopes also requires strict wavefront sensing accuracy and adaptive control to maintain path lengths between the segments. We have already reached the present limit of practical technology in the manufacturing of large single-mirror telescopes; even larger apertures will require path length control that goes beyond segment edge matching and explicitly examines errors between widely separated portions of the pupil. This requires wavefront sensing with the full beacon spatial coherence, which is already offered by PyWFSs and is available with the HyWFS. An extreme example is the recent proposal by the Breakthrough Starshot initiative to send miniaturized spacecraft to our neighboring star system Proxima Centauri using laser light as the propellant.[3] This will require cophasing an array larger than 4 km in diameter, comprising millions of small telescope apertures projecting the laser beams such that constructive interference will occur at the spacecraft's light sail outside of Earth's atmosphere.[4,5] Arrays of telescopes such as this will require inexpensive wavefront sensing with high dynamic range and sensitivity. We note that in this instance, spatial coherence over the full aperture cannot be expected from natural starlight because of the typical angular subtense of stars bright enough to act as beacons. A laser beacon mounted on the spacecraft mothership, however, can certainly remain unresolved at the launch aperture, and is still preferred because of the lack of suitably bright stars in the vicinity of Proxima Cen.

Guthery and Hart describe simulations of the expected performance and relative operating regimes of the HyWFS.[1] The results are illustrated in Figure 1. For weak aberrations the PyWFS mode corrects with lower

residual error until the PyWFS saturates. Once saturation occurs, which is in the same regime as the standard unmodulated PyWFS, the SHWFS mode is better at reconstructing the wavefront. As in the standard SHWFS, the dynamic range is limited only by the field of view of the subapertures. To verify the results of these simulations, a simple laboratory test has been designed according to the floating optic illustration of the system shown in Figure 2. The design has been implemented primarily from commercially available components as an inexpensive prototype.

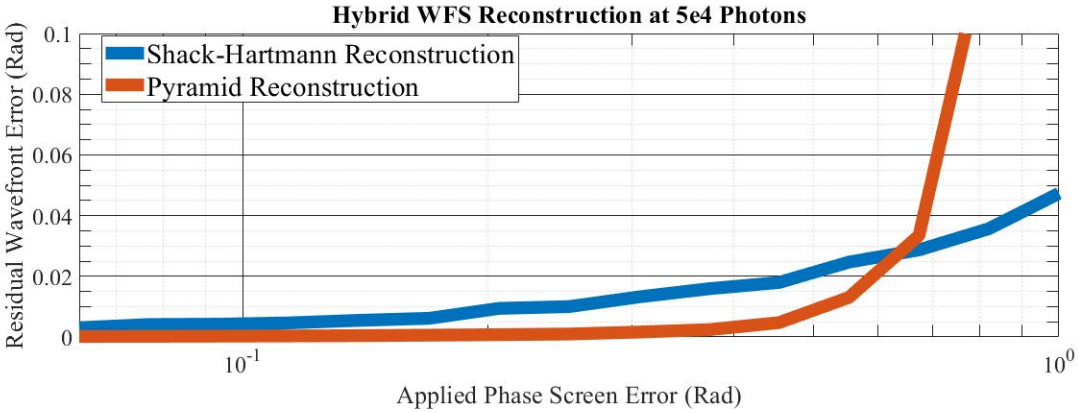

Figure 1. Simulation results for the pyramid and Shack-Hartmann modes of the HyWFS generated by Guthery and Hart. There is a clear point at which the PyWFS mode saturates as the wavefront error grows, indicating where the system would switch to the SHWFS mode.

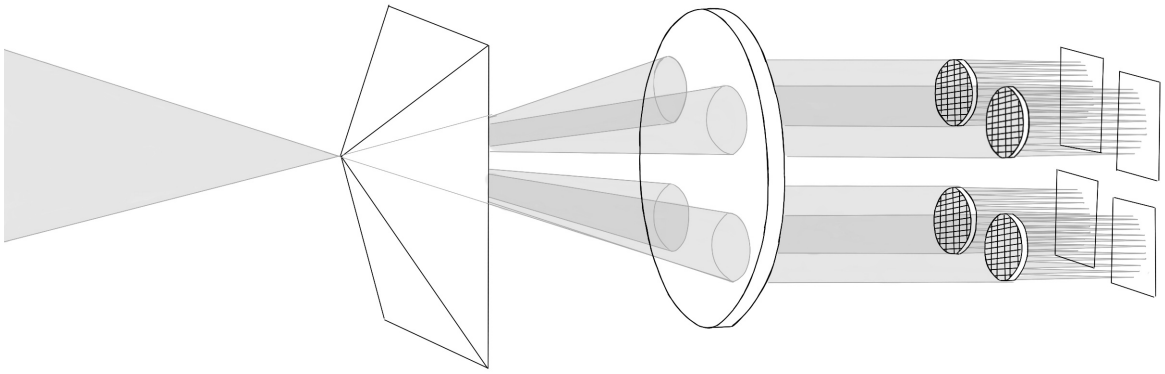

Figure 2. Simple illustration of the HyWFS optical system. The pyramid prism generates four diverging beams which are then collimated to form pupil images on a lenslet array. The lenslets focus the beacon onto a detector to form four Shack-Hartmann-looking spot patterns.

2. HYBRID WAVEFRONT SENSOR DESIGN

The bench top prototype is intended to validate the simulated results in Figure 2 within the constraint of a limited budget. This section describes the overall architecture of the HyWFS as well as the specific optical and mechanical parameters used to reach the design goal. The broad optical architecture is diagrammed in Figure 3. The final system parameters are in Table 1 at the end of the section 2.3.

Calibration of the HyWFS relies on a DM placed at the entrance pupil of the system to introduce known aberrations. The DM is embedded in a bench top AO system used for instructional purposes, but in this instance was used only to measure the HyWFS influence functions and then to carry out open-loop performance tests.

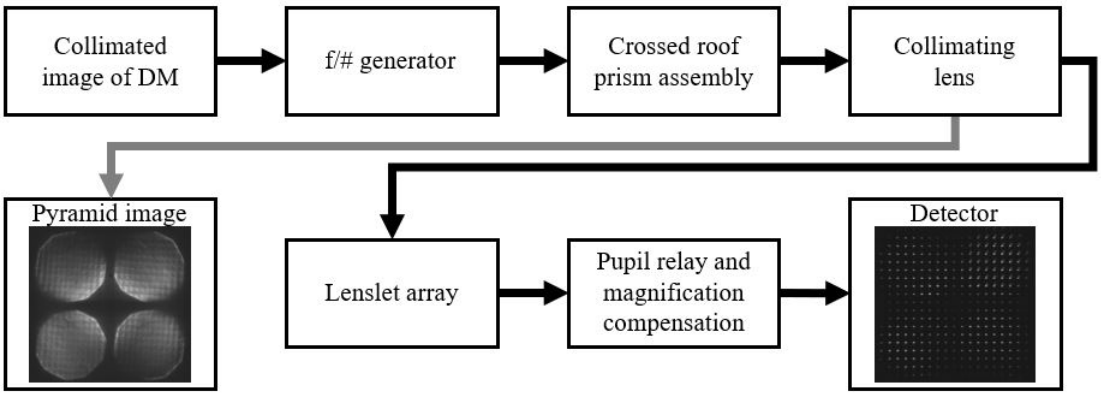

Figure 3. Broad optical architecture of the HyWFS designating flow of light through the system and the order of the components. The intermediate pyramid image is shown for reference but is not part of the completed system. The final image shown is an unaberrated HyWFS image captured by the detector in the final system.

2.1 Detector

A FLIR Grasshopper GS3-U3-23S6M-C already in-house was used as the detector to initially constrain the system scale and geometry. The rest of the design was set to easily couple the pupil images and resulting Shack-Hartmann spots to the available detector with proper magnification and image plane conjugation. Testing and verifying the HyWFS performance is done in open loop; therefore, sensor speed and response are not addressed.

2.2 Lenslet array

To ease computational complexity, the lenslet array was designed so that the subaperture size was an integer number of pixels on the detector. The detector has 5.86 µm pixels in a 1920×1200 pixel grid. After considering the size of the detector and the dimensions of most lenslet arrays, lenslet subapertures were set at 32×32 detector pixels. Each effective quad-cell pixel is therefore 16×16 detector pixels. Limiting pupil separation is also beneficial if detector uniformity is a concern, resulting in the decision to separate each pyramid pupil image by just a single Shack-Hartmann lenslet subaperture. The resulting lenslet subapertures are 187.5×187.5 µm on a 19×19 lenslet subaperture grid. Each pupil image occupies 8×8 lenslet subapertures with one lenslet spacing between each pupil image and two additional lenslets around the border of the array.

The array was manufactured by diamond turning in the Precision Freeform Optics Design, Fabrication and Testing Facility at the University of Arizona. The capabilities of the facility allowed for the subapertures to be squares with close to 100% fill factor.

2.3 Verifying pupil geometry

Geometric analysis of the system components shows that there are five variables to control pupil separation and pupil size on the image plane: the f/# of the beam entering the system focusing onto the prism tip, the focal length of the collimation lens, the thickness of the prism along the optical axis, the index of refraction of the prism, and the angle of the prism faces. The pyramid prism geometry, f/# generator at the WFS entrance

pupil, and collimating lens were constrained together to match the dimensions of the system. By constraining the prism thickness to 10.5 mm and choosing BK7 as the prism material, the remaining system parameters were determined by mechanical tolerances and the predetermined image geometry.

2.3.1 Crossed roof prisms

Pyramid prism costs were reduced by using a crossed roof prism design. The left side of Figure 4 indicates how two crossed roof prisms geometrically perform the same task as a single pyramid prism. Previous work has shown that the crossed roof prism design results in minimal impact on the performance of the PyWFS.[6,7]

Roof prisms are easier to manufacture than three- or four-sided pyramids because only two faces are ground to a common edge. In addition, the centration of the roof edge with respect to the prism sides is not held to a tight tolerance. Misalignment in centration of the prism roof edges is easily compensated with basic mounting schemes. This makes the crossed roof prism less expensive and faster to manufacture than three- or four-sided pyramid prisms while being easier to align. We refer to the crossed roof edges as the 'prism tip' throughout the rest of this paper.

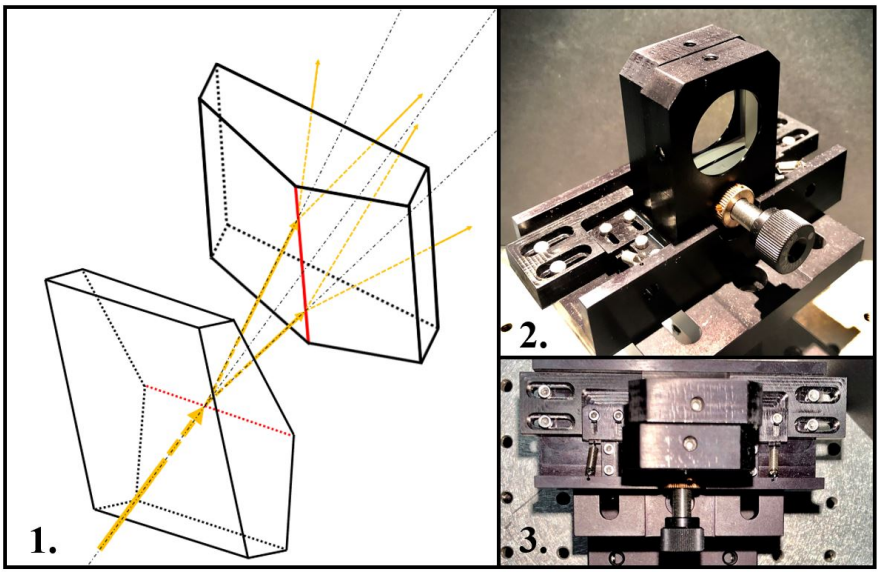

Figure 4. 1) Illustration of how a crossed roof prism serves to split light identically to a pyramid prism to produce 4 pupils. The roof angle, beam deviations, and prism spacing have been exaggerated. The roof edges are in red and are perpendicular to each other. 2) side view of the custom prism mount used in the HyWFS along with the prisms mounted. 3) Overhead view of the custom prism mount showing how it is constrained.

2.3.2 Input beam focal ratio

To avoid blurring in the pupil images, it is essential that the beam is focused at the prism tip. Furthermore, the distance between the roof edges must be small compared to the Rayleigh range of the focused beam. Ideally, the roof edges would be in contact. However, contacting the edges would cause damage to the optical quality roof edge resulting in light scatter and point-spread function corruption at the prism tip. The beam is approximately collimated inside the Rayleigh range, which is desirable in constraining the system geometry, assuring that the center-to-center pupil image separation will be almost identical in the tangential and sagittal planes as seen at the detector. Section 2.4 describes the prism mounting scheme in detail.

The size of the focused spot must be large compared to the manufactured width tolerance of the prism roof edges. If the focused spot is smaller or comparable in size to the edge width, most of the light will be scattered out of the beam and not contribute to useful signal at the detector. To ensure that the spot is large compared to the mechanical edge of the prism, the light must be brought to focus at a sufficiently high focal ratio. A ratio greater than f/80 was required in view of the prism manufacturer's expected mechanical specifications on the

roof prism edge size and tolerance. Since the depth of focus also scales with f/#, a larger value also loosens alignment tolerances, which is desirable. Boundlessly increasing the f/# is not beneficial, however, as high spatial frequencies are lost from the PSF and the system grows in physical length.

The beam entering the HyWFS entrance pupil is collimated. At the entrance pupil, an inexpensive commercially available doublet generates a focal ratio of f/84 at the prism tip. An adjustable iris served as the aperture stop. The depth of focus of the beam, $\sim$ 7 mm in visible light, is much larger than the separation of the two prism roof edges, held at a maximum separation of 50 µm. This satisfies the criterion for the crossed prisms to function effectively as a pyramid.

2.3.3 Collimating lens and prism

The pupil diameter and relative spacing are driven by the focal length of the collimating lens and the roof angle of the prisms respectively. The collimating lens was selected as a commercially available part, a Newport PAC076 125 mm focal length triplet. Triplet lenses have low aberration content and symmetric principle planes, both of which are desirable traits to have when modeling and aligning. Custom prisms were made with a roof angle of 0.748° measured from the tangent line of the prism tip–a line parallel to the planar optical face of the prism–to each of the slanted faces of the prism. The prism angle solution was found in a Matlab geometric model and then verified in a Zemax model.

Table 1. Final design parameters for each component of the HyWFS.

f/# generator	
Achromatic lens focal length	300 mm
Entrance pupil diameter	3.57 mm
Roof prisms	
Material	BK7 (n = 1.517)
AR coating	λ = 400-700 nm
Roof angle	0.748°
Collimating lens	
Triplet lens focal length	125 mm
Lenslet array	
Lenslet side lengths	187.5×187.5 µm
Lenslet focal length	1.5 mm
Grid size	19x19 lenslets
Lenslet focus relay optics	
Relay magnification	-1
Image plane properties	
Pixel size	5.86 µm
Detector size	1920×1200 pixels
Pyramid pupil image diameter	256×256 pixels
Shack-Hartmann pupil image diameter	32×32 pixels

2.4 System assembly

System parameters were determined while continuously considering the physical assembly of the system. As previously mentioned, an instructional AO kit with a DM was decoupled from its native wavefront sensor and the DM pupil image was relayed to the entrance pupil of the HyWFS, effectively making the AO kit a test bed. This was kept in mind when determining the scale of the system. The full system layout is shown in Figure 5.

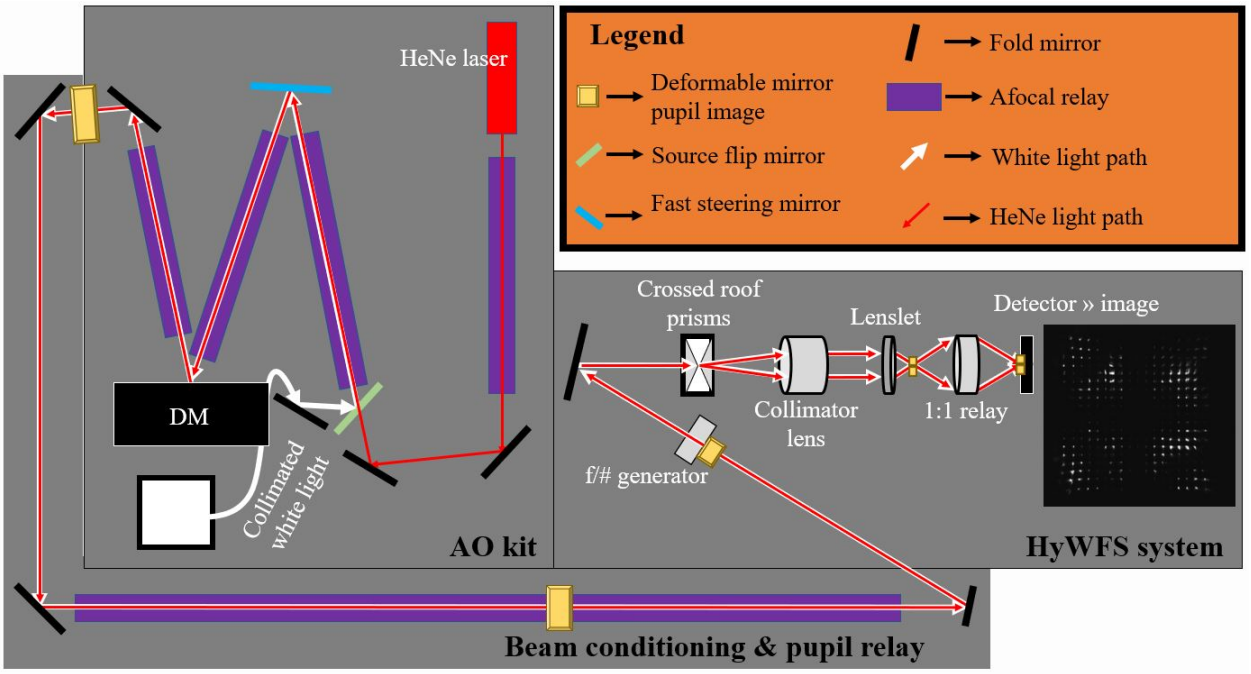

Figure 5. Full system layout of the HyWFS integrated with the AO kit such that the DM can send aberrated wavefronts into the wavefront sensor using either white light or red HeNe laser light.

Mounting capabilities are also a powerful design constraint and are used in the HyWFS design process. The most influential mounting constraint for the HyWFS is the crossed roof prism mount. The loose tolerance requirements for all other system optics allows for the use of generic commercially available mounts.

2.4.1 Crossed roof prism mount

As discussed in section 2.3.2, the prisms are brought within 50 µm of each other without the edges contacting. This is achievable with a custom mount using standard manufacturing tolerances for aluminum parts. The prism mount is shown in the right panels of Figure 4. The prism mount in the foreground of the top right image of Figure 4 has a micrometer threaded through the base, contacting the back prism mount on the roof edge side. The distant prism mount has springs that pull it towards the first prism face. The only component stopping the prism edges from contacting is the micrometer. This can be observed in the bottom right image of Figure 4.

Starting with the prisms safely spaced apart, the micrometer is slowly adjusted until the mechanical edges of the prism mounts are at the desired separation given the mechanical tolerances of all the components being used. An alignment telescope mounted to a micrometer focused on the edges of the prism mounts as the measurement tool to determine the mechanical edge separation of the two mount faces. To use the mechanical edges of the mount as the measurement datum, the distance from the prism roof edge to the mechanical mount edge must be known. This distance should be measured before mount assembly. Alternatively, the prism mount can be designed so that when the mechanical faces of the mount are in contact the prism roof edges are at the proper spacing. The method of mounting other system optics was determined for each element depending on which elements needed fine adjustment.

2.4.2 Alignment

The height and lateral position of the crossed roof prism assembly was fixed and used as the height and lateral position datum of the entire HyWFS. The rest of the system is aligned to the fixed height of the prism tip. The prism assembly was mounted on a ThorLabs PT1B translation stage to adjust the prism tip location along the optical axis. This is important to assist alignment of the focused spot from the f/# generator. The rest of the system was built on ThorLabs universal post holders and dovetail translation stages if fine adjustment was

necessary. Once the input beam was properly aligned with the f/# generator to focus onto the prism tip to generate four pupils, each element in the optical train was placed in the order the light interacts with it in the system. Alignment of these elements was performed using posts and iris to establish lateral position and height datum. Final images of the HyWFS image plane can be seen in Figure 6.

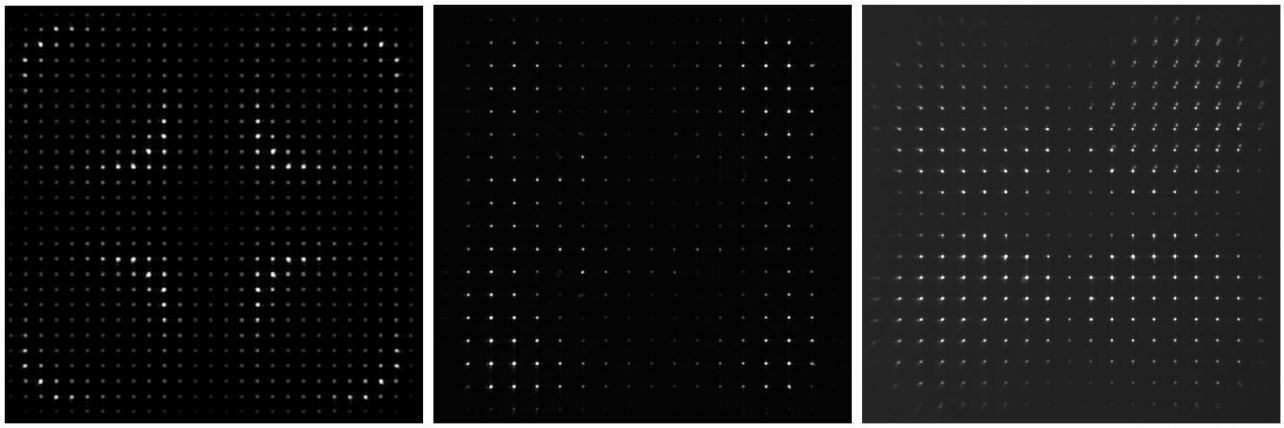

Figure 6. Left: Simulated image plane for a HyWFS from Guthery and Hart. Center: HyWFS image plane when using HeNe laser light. Right: HyWFS image plane using a broadband white light source.

3. SYSTEM TESTING

Testing of the HyWFS consists of two parts. Initial testing verifies that the designed and built system is capable of replicating a test comparable to the simulated environment of Guthery and Hart. This involves confirming HyWFS image outputs and DM control. Subsequently a final test is performed with an automated process developed to replicate the simulated environment. Only the initial testing of the HyWFS system is covered in this paper while a proposed final test is outlined.

3.1 Initial testing

To confirm that the bench top prototype is capable of producing a comparable test environment as in simulation, a series of system capabilities have to be operating correctly. The output HyWFS images should look as we expect given proper alignment. A process to impart known phase aberration maps with the DM onto the input wavefront has to be understood and repeatable. Real HyWFS image test data suitable for optimizing the wavefront reconstruction software must also be obtained. Once hybrid images are being produced, the quality of the output images can be assessed and system improvements can be identified for the final test environment.

3.1.1 Deformable mirror phase maps

The DM is a Boston Micromachines (BMC) 12×12 actuator MEMS device. ThorLabs provides an AO software suite with their kits that allows for control of the BMC DM with text files delimited in column by spaces and delimited in row by returns. The text file must be saved to a .spf file extension. Zernike DM shape files are generated with a Matlab routine that takes 12×12 matrices of the modes and formats them as the properly delimited text files with the .spf extension. The amplitudes of the modes are normalized and then scaled to specified fractions of the DM poke before being turned into text files. The same routine in Matlab can turn 12×12 Kolmogorov phase matrices into .spf files that can be read onto the DM. Example images of modes applied to the DM as seen by the HyWFS are in Figure 7.

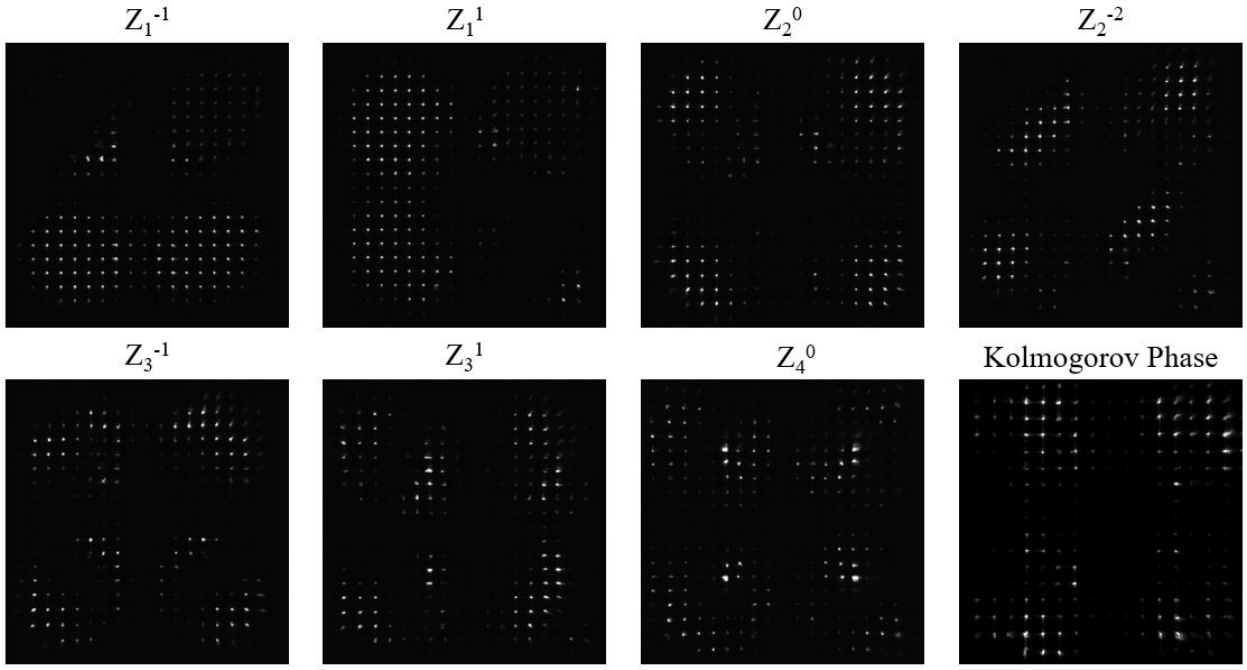

Figure 7. Output HyWFS images for different DM shapes. The individual Zernike modes have scaled peak to valley amplitudes of 75% the maximum poke of the DM actuators and were generated with white light. The Kolmogorov phase map has a peak to valley amplitude of the maximum DM poke and was generated with HeNe laser light.

3.1.2 Output image analysis

Initial testing is predominantly quantitative and verifies that the designed and built system is producing the images we expect. It also acts as a source of real data to be used while refining software that performs the data reduction of hybrid images as discussed by Guthery and Hart. The system test bed setup initially described in Section 2 is coupled to the AO kit, which proved to be too unreliable since the AO kit is used for other purposes than as a HyWFS test bed. Additionally, coupling the white light into the AO kit was not optimal due to the fixed AO kit geometry and limited working room. The white light had to be brought into the system from above which resulted in low-signal elliptical beams given the equipment available to the lab. The fast steering mirror in the AO kit serves no purpose for the HyWFS test bed and was introducing drift errors over long aligning and testing periods. The solution is to create a dedicated test bed for the HyWFS. Using a kinematic base plate for the DM in the AO kit as well as in a new HyWFS test bed allows for the same DM to be used in both systems independently.

A stand alone test bed with sources exclusive to the HyWFS system has been constructed. Baffling has also been placed around the HyWFS optics to prevent ghost spots – these spots can be seen in Figure 7 in the top right pupil of the white light images. Band pass filters are placed in the white light source path to more closely simulate on-sky guide star observation wavebands. The new system layout is shown in Figure 8.

3.2 Proposed final test

Recreating the tests of Guthery and Hart requires that hundreds of known Kolmogorov phase maps are applied to the DM and subsequently imaged by the HyWFS. The images must then be used to reconstruct the wavefront using both the SHWFS and PyWFS partitions. Finally, the reconstructed modes must be compared to the known Kolmogorov phase maps to extract the residual wavefront error. Plotting the reduced data as a function of the strength of the Kolmogorov phase error would produce a plot comparable to Figure 1. This is the initial goal of the paper and will be completed using the new system layout.

To get a complete understanding of the built HyWFS system performance to compare with theory, the testing routine must be reiterated as a function of photon signal on the detector as well as for both monochromatic

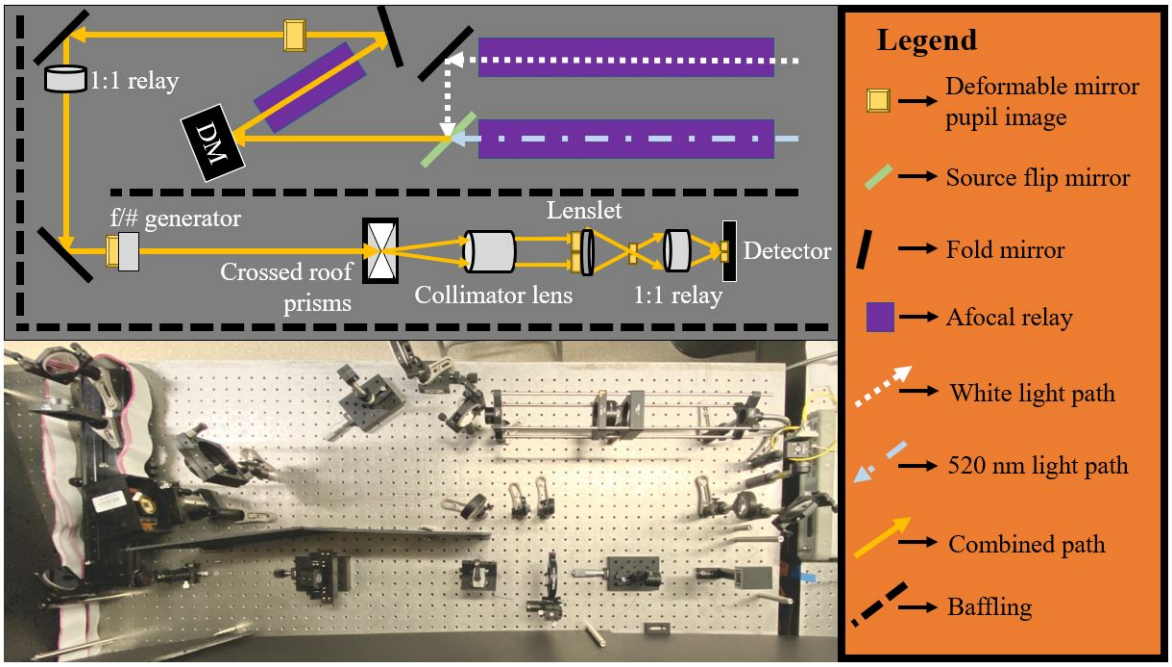

Figure 8. New system layout with dedicated sources and baffling. The physical system (currently being aligned) is in the image at the bottom while a diagrammatic illustration of the system with identical parity is above.

light and polychromatic light of different band passes. This requires that the testing become automated due to the volume of data that must be obtained. This can be accomplished with a Matlab routine that generates Kolmogorov phase maps, applies them to the DM, and then takes an image of the DM with the HyWFS detector. This functionality is already operating in the HyWFS test bed. For the final system test, the automatic DM phase map and image capturing routine will iterate and the output image will be reduced after it has been captured. The reconstructed wavefront residuals from both the SHWFS and PyWFS partitions will be determined and stored before moving on to a newly generated Kolmogorov phase map. For a given wavelength source and flux transmission, this process will be repeated for the desired number of Kolmogorov phase maps. Source wavelength and flux transmission can then be varied for a either identical or new Kolmogorov phase maps. This will enable fast physical testing to properly recreate the results of Guthery and Hart in their simulation.

4. CONCLUSIONS AND FUTURE WORK

The HyWFS system has been successfully built at a low cost. The bench top setup captures aberrated wavefronts generated by the AO kit DM in the form of hybrid images. These images consist of four pupils broken into a grid of focused spots as was theorized by Guthery and Hart. Test images have been obtained to refine wavefront reconstruction software. Full quantitative characterization of the system will be completed with a final system test.

The test bed design for the final system test of the HyWFS has been completed and is currently undergoing alignment at The University of Arizona. This test bed will approximately recreate the simulated environment of Guthery and Hart. Final testing will automatically generate and apply Kolmogorov phase maps to the DM, then reduce those images with both the system SHWFS and PyWFS partitions. The reconstructed wavefront residual error for both partitions will be measured as a function of aberration strength in the Kolmogorov phase map for a series of different source photon signals and for different source wavelengths.

Improvement of current wavefront sensing capabilities is becoming increasingly more important as science goals in astronomy, medical, and defense fields are more frequently requiring adaptive optics. The effect of improving this technology is amplified if wavefront sensing capabilities improve without a nominal increase in cost or system complexity. Verification of HyWFS theory with a physical system has proven to be relatively

inexpensive thus far. This is aided by the use of crossed roof prisms as a pyramid prism substitute. Removing the need for moving parts to modulate the beam around the prism tip also aids in reducing cost and complexity. We expect the HyWFS to offer high dynamic range and high sensitivity at a relatively low cost in a simple architecture.

REFERENCES

[1] Guthery, C. E. and Hart, M., "Theory and design of a hybrid wave-front sensor for adaptive optics," *Adaptive Optics for Extremely Large Telescopes 6* (2019).

[2] Ragazzoni, R., "Pupil plane wavefront sensing with an oscillating prism," *Journal of Modern Optics* **43**(2), 289–293 (1996).

[3] Parkin, K., "The breakthrough starshot system model," *Acta Astronautica* **152**, 370–384 (2018).

[4] Lubin, P., "A roadmap to interstellar flight," *Journal of the British Interplanetary Society* **69** (2016).

[5] Hughes, G., Lubin, P., Griswold, J., Cook, B. V., Bozzini, D., O'Neill, H., Meinhold, P., Suen, J., Bible, J., Riley, J., Johansson, I., Pryor, M., and Kangas, M., "Optical modeling for a laser phased-array directed energy system," *Proceedings of SPIE - Nanophotonics and Macrophotonics for Space Environments VIII* **9226** (2014).

[6] Engler, B., Weddell, S., and Clare, R., "Wavefront sensing with prisms for astronomical imaging with adaptive optics," *2017 International Conference on Image and Vision Computing New Zealand (IVCNZ)* , 1–7 (2017).

[7] van Kooten, M., Véran, J.-P., and Bradley, C., "Alternative pyramid wavefront sensors," *Journal of Astronomical Telescopes, Instruments, and Systems* **3**(2), 1 – 6 – 6 (2017).